AD-A121 564 A CODE FOR THE SECONDARY ELECTRON ENERGY DISTRIBUTION IN AIR AND SOME APPLICATIONS(U) NAVAL RESEARCH LAB WASHINGTON DC D J STRICKLAND ET AL. 18 NOV 82 1/1

UNCLASSIFIED NRL-MR-4956 F/G 20/8. NL

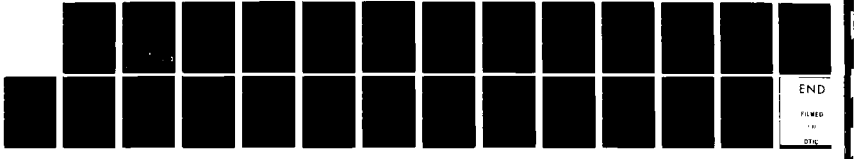

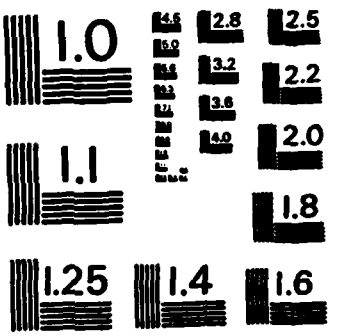

NRL Memorandum Report 4956

A Code for the Secondary Electron Energy Distribution in Air and Some Applications

D. J. STRICKLAND

Beers Associates
Reston, VA 22090

A. W. ALI

Plasma Physics Division

November 18, 1982

This report was sponsored by Defense Advanced Research Projects Agency (DoD), DARPA Order No. 3718, monitored by NSWC under Contract No. N60921-81-WR-W0190.

NAVAL RESEARCH LABORATORY
Washington, D.C.

SECURITY CLASSIFICATION OF THIS PAGE (When Data Entered)

REPORT DOCUMENTATION PAGE		READ INSTRUCTIONS BEFORE COMPLETING FORM
1. REPORT NUMBER NRL Memorandum Report 4956	2. GOVT ACCESSION NO. AD-A121564	3. RECIPIENT'S CATALOG NUMBER
4. TITLE (and Subtitle) A CODE FOR THE SECONDARY ELECTRON ENERGY DISTRIBUTION IN AIR AND SOME APPLICATIONS		5. TYPE OF REPORT & PERIOD COVERED Interim report on a continuing NRL problem. 6. PERFORMING ORG. REPORT NUMBER
7. AUTHOR(s) D. J. Strickland* and A. W. Ali		8. CONTRACT OR GRANT NUMBER(s)
9. PERFORMING ORGANIZATION NAME AND ADDRESS Naval Research Laboratory Washington, DC 20375		10. PROGRAM ELEMENT, PROJECT, TASK AREA & WORK UNIT NUMBERS 61101E; 47-0900-0-2
11. CONTROLLING OFFICE NAME AND ADDRESS Defense Advanced Research Projects Agency Arlington, VA 22209		12. REPORT DATE November 18, 1982 13. NUMBER OF PAGES 24
14. MONITORING AGENCY NAME & ADDRESS(if different from Controlling Office) Naval Surface Weapons Center Silver Spring, MD 20910		15. SECURITY CLASS. (of this report) UNCLASSIFIED 15a. DECLASSIFICATION/DOWNGRADING SCHEDULE

16. DISTRIBUTION STATEMENT (of this Report)

Approved for public release; distribution unlimited.

17. DISTRIBUTION STATEMENT (of the abstract entered in Block 20, if different from Report)

18. SUPPLEMENTARY NOTES

*Present address: Beers Associates, Reston, VA 22090.

This report was sponsored by Defense Advanced Research Projects Agency, (DoD), DARPA Order No. 3718, monitored by NSWC under Contract No. N60921-81-WR-W0190.

19. KEY WORDS (Continue on reverse side if necessary and identify by block number)

Energy deposition
Secondary electron distribution
Air ionization
Energy per ion pair

20. ABSTRACT (Continue on reverse side if necessary and identify by block number)

The development and some applications of a secondary electron distribution code (SED) is discussed in detail. An (SED) code is essential for high energy electron beam deposition in the atmosphere. The code provides the secondary electron flux, the energy flow into various ionizations, excitations and the fractional contributions of the primary and the secondary electrons to these processes. The code predicts a 34 eV per ion pair expenditure and various ion fractions per ion pair which are in good agreement with the accepted values.

DD FORM 1 JAN 73 1473 EDITION OF 1 NOV 65 IS OBSOLETE
S/N 0102-014-6601

SECURITY CLASSIFICATION OF THIS PAGE (When Data Entered)

CONTENTS

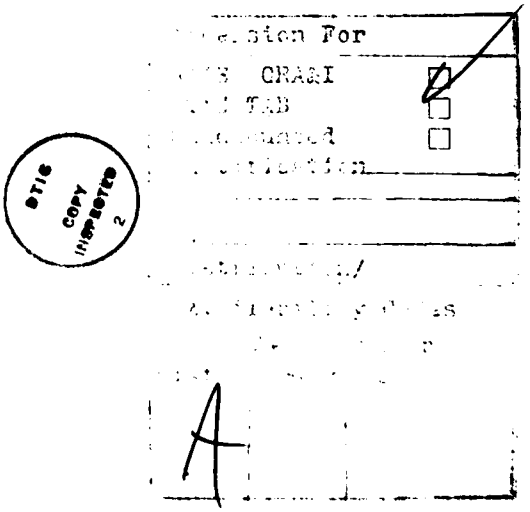

A CODE FOR THE SECONDARY ELECTRON ENERGY DISTRIBUTION IN AIR AND SOME APPLICATIONS

1. INTRODUCTION

The interaction of high energy electrons (>1 KeV) with atoms and molecules, the generation of the secondary electrons and their subsequent energy degradation is a subject of great interest in many areas of applied physics. Among these areas are: precipitation of energetic electrons in the upper atmosphere resulting in auroral phenomena, production of laser radiation by high energy-high current electron beams, and electron beam generated discharges.

Various methods have been utilized to address the electron energy deposition problem. These may be classified in different ways depending on one's emphasis. Major classifications are as follows: 1) Transport versus local descriptions, 2) Continuous slowing down approximation (CSDA) versus discrete energy loss description (DEL), and 3) Transport or local energy loss equation versus Monte Carlo approach. There is an extensive literature on this subject as it relates to applications cited above. Here we will just note some of the works representative of past efforts. Green and his colleagues[1,2,3] have approached the problem through the continuous slowing down approximation and have applied their calculations to auroral phenomena as well as deposition in other gaseous media. The continuous slowing down approximation has been improved to include discrete energy loss for electrons with energies below 500eV and has been applied to auroral phenomena [4,5] as well as other gaseous elements[6-8]. Monte Carlo[9] and Fokker-Planck[10] methods have also been utilized to calculate the energy deposition as well as the spatial distribution of primary elctrons. The steady state forms of the Boltzmann equation provide another method[11,12,13] to calculate the equilibrium distribution of the secondary electrons.

Manuscript approved September 30, 1982.

In this work, we are specifically interested in detailed energy partitioning in air during and following the passage of a high energy electron beam through the air. For this purpose we have developed Code SED which provides a discrete energy loss description for specification of the secondary electron distribution function. The approach is basically that given in reference 11 but limited to local deposition. This code has been coupled to a time dependent air chemistry code[14] (CHMAIR-II) which describes the many effects on neutral and ionized species during and following electron beam deposition. In this report, however, we limit our discussions to the secondary electron distribution obtained using code SED.

2. APPROACH

We wish to specify the quantity $n_e(E,t)$ which is the density of secondary electrons per unit volume per unit energy ($cm^{-3}eV^{-1}$). Given n_e, we may obtain various production rates of interest given by P:

$$P(t) = n \int n_e(E,t)\ v(E)\ \sigma\ (E)\ dE \qquad cm^{-3} \cdot sec^{-1} \qquad (1)$$

where n is the density of the target species and σ is the electron impact cross section. Most of the contributions to P comes from below 100 eV and for this reason we restrict ourselves to low energies for which transport effects are unimportant.

The density n_e is specified using

$$\frac{\partial n_e}{\partial t} = S(E,t) - \sum_{\ell} n_\ell \sigma_\ell (E) v(E) n_e(E,t) + \sum_{\ell} n_\ell \sum_{k} \int \sigma_{\ell k} (E', E) v(E') n_e(E', t) dE' + n_p (t) \frac{\partial}{\partial E} \left[L_p (E) v(E) n_e(E,t) \right] \quad (2)$$

where S is the volume production rate in e/cm^3-s-eV, n_ℓ is the ℓ^{th} species causing energy loss, the σ's are energy loss cross sections, n_p is the plasma density, and L_p is the loss function for loss to the plasma electrons. The species treated in this equation are N_2 and O_2. The electrons lose but do not gain energy in the description, thus allowing us to obtain n_e one energy at a time starting at the high energy end. The energy dependence of n_e within the integral is specified in a manner similar to that used by Strickland, et al[11].

3. SPECIFICATION OF S(E,t)

The secondary electron volume production rate S(E,t) is given by

$$S(E,t) = j_b(E_b) \sum_{\ell} n_\ell \sigma_e (E_b, E) \quad (3)$$

where j_b is the beam current density in $e \cdot cm^{-2} \cdot s^{-1}$ and $\sigma_\ell (E_b, E)$ is the differential ionization cross section for species ℓ. We use the expression by Porter, et al[3] for this cross section which is similar to the Moeller[15] formula for large momentum transfer values. Figure 1 shows the differential ionization cross section of N_2 from 1 to 1000eV for E_b = 1 MeV. The Moeller[15] cross section is included to compare with the Porter expression at large E_s values where both are in close agreement.

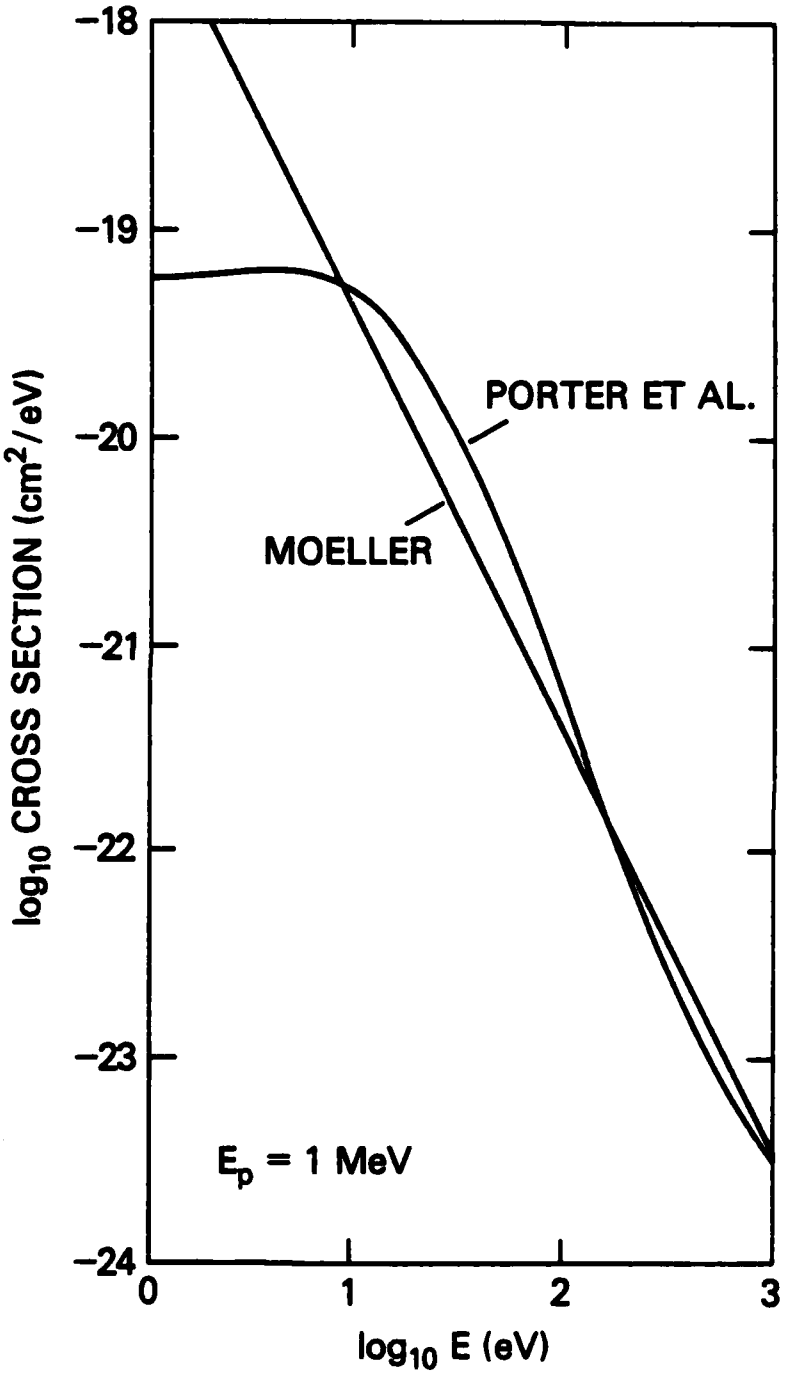

Fig. 1 — Differential ionization cross section for 1 MeV electrons impacting N_2

4. ELECTRON IMPACT CROSS SECTIONS

In the discrete energy loss description, cross sections are required for all important inelastic scatterings. This amounts to approximately ten cross sections per species, most of which apply to the process of excitation. Ionization accounts for the remaining cross sections. For excitation, $\sigma_{\ell k}(E',E)$ may be expressed as

$$\sigma_{\ell k}(E',E) = \sigma_{\ell k}(E') \; \delta\left[E' - (E+W_{\ell k})\right] \tag{4}$$

where the delta function restricts energy loss to the excitation energy $W_{\ell k}$. For ionization, we use the form

$$\sigma_{\ell k}(E',E) = \sigma_{\ell k}(E') \; p(E',E) \tag{5}$$

where $\sigma_{\ell k}(E')$ is the total ionization cross section in cm^2 for ion state k and p is a function with normalization

$$\int_0^{(E'-W_k)/2} p(E',E) \; dE = 1 \; . \tag{6}$$

The integration is over the secondary electron energy defined to be the lesser of the energies of the two electrons emerging from an ionization event. The form of p is chosen to be that used by Strickland, et al[11].

The individual cross sections will not be presented here. They can be found, however, in a recent compilation by Ali[16]. The total cross section for each species may be seen, however, in Figure 2. The N_2 feature peaking at 2.5 eV results from vibrational excitation of the ground state. This single feature is actually composed[16] of eight cross sections for excitation through vibrational level v" = 8. The minimum in the N_2 cross section near 6 eV will

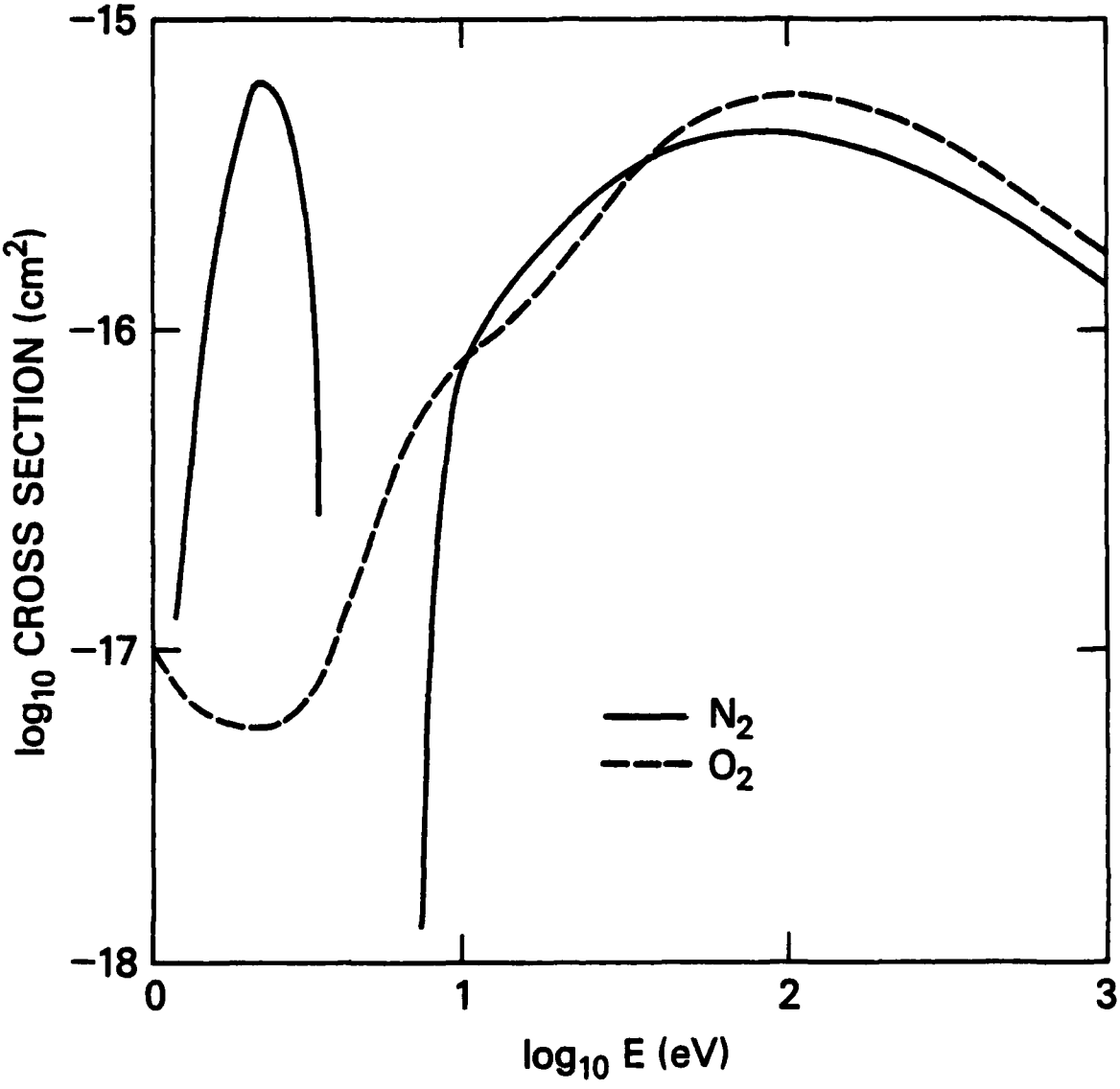

Fig. 2 — Total inelastic electron impact cross sections for N_2 and O_2

be seen to have a noticeable effect on the secondary electron distribution near this energy. The distribution takes on large values in this region since electrons find themselves trapped in velocity space for a time due to the small inelastic collision frequency.

5. ENERGY LOSS TO THE PLASMA ELECTRONS

Equation (2) includes an expression for energy loss to the plasma electrons. This term becomes important for low energy secondaries especially when fewer electronic state excitation processes occur with decreasing energy. For L_p, we are using the following expressions from Schunk and Hays[17]

$$L_p(E) = \frac{1.3 \times 10^{-13}}{E} \ln \frac{8.2 \times 10^9 \, E^{1.5}}{n_p^2}, \qquad E < 20 \text{ eV} \tag{7}$$

$$= \frac{1.3 \times 10^{-13}}{E} \ln \frac{5.4 \times 10^{10}}{n_p^2} E, \quad E > 20 \text{ eV} \tag{8}$$

The plasma electron density n_p appears explicitly in the plasma loss term in equation (2) and in L_p above. For our time dependent results, n_p is calculated self-consistently along with n_e. For our steady state results to be presented below, n_p is simply an input parameter to the calculations.

6. MATRIX APPROXIMATION TO THE SECONDARY ELECTRON EQUATION

Equation (2) can be written as

$$\frac{\partial n_{e_i}}{dt} = P_i - \ell_i \tag{9}$$

where P_i and ℓ_i are the volume production and loss rates for species i. In the case of secondary electrons, the index i refers to energy E. To arrive at

Equation (9), approximations must be made to the integral and plasma loss terms in Equation (2). This is done by first specifying an energy grid over the range of interest. The density n_e within the integral is then given a quadratic dependence over a given energy zone following the method of Strickland, et al[11]. This leads to replacement of the integral by a sum of terms of the form

$$\sum_{\ell} n_{\ell} \sum_{j=1}^{i} R_{ij}^{\ell} n_{ej}$$

For the plasma term, one sided, finite differencing is used over the interval (E_i, E_{i-1}) where E_{i-1} is greater than E_i. Equation (2) may then be expressed in the form

$$\frac{\partial n_{ei}}{\partial t} = -\left(\sum_{\ell} n_{\ell} R_{ii}^{\ell} + n_p \frac{L_{pi}}{\Delta E_i} v_i\right) n_{ei}$$

$$+ \sum_{\ell} n_{\ell} \sum_{j=1}^{i-1} R_{ij}^{\ell} n_{ej} + n_p \frac{L_{p,i-1} v_{i-1}}{\Delta E_i} n_{e,i-1} \qquad (10)$$

$$+ S_i$$

The matrix element R_{ij}^{ℓ} is obtained from combinations of terms whose integral parts have the form

$$\int_{E_j}^{E_{j-1}} \sigma_{\ell k}(E',E)\, v(E')\, f(E')\, dE'$$

where $f(E')$ is either $\ln^2 E'$, $\ln E'$, or 1.

7. ENERGY CONSERVATION

Two tests have been applied to our solution of Equation (10) in steady state. The first determines how well $n_e(t)$ conserves energy and in the second, we calculate the energy expended to generate an ion pair, ΔW_{ip}. The

accepted value of ΔW_{ip} for air is ~ 35 eV/ion pair. The conservation test determines how well the following equality holds:

$$\sum_{\ell,k} W_{\ell k} P_{\ell k} + n_p \int L_p(E)\, v\, n_e(E)\, dE = \int S(E)\, E\, dE \qquad (11)$$

The conservation principle states that the rate of energy transferred to the ion and excited states and to the plasma equals the rate of energy going into the secondary electron spectrum. The production terms $P_{\ell k}$ refer only to production by secondary electrons. We find that the solution $n_e(E)$ leads to less than 10% error in satisfying Eq. (11).

For ΔW_{ip}, we are obtaining a value of between 34 and 36 which agrees well with the accepted value. To calculate ΔW_{ip}, we first determine how much energy is deposited in a unit volume per unit time by passage of the primary electrons through it. The Porter[3] cross section is used to give the total primary ionization rate which in turn gives the energy going into potential energy of the ion states. This same cross section gives S, which when multiplied by E and then integrated gives the rest of the beam energy loss by ionization. There is also energy loss to excited states. Based on cross sections in the keV regime, the number of excitation events will be similar to the number of ionization events caused by direct beam electron impact. This provides us with the loss due to excitation once given the average excitation energy threshold.

The other quantity needed to specify ΔW_{ip} is the total number of ion pairs produced by the beam energy loss. The integral of S(E) gives the number produced by direct beam ionization. Equation (2) gives the number of ion pairs by all generations of secondary electrons for each ionization process. Summing over processes and adding the result to the direct beam contribution gives the desired result.

8. RESULTS AND DISCUSSION

The problem being addressed is the incremental energy loss of an electron beam on its passage through some thickness δs . We wish to know how the deposited energy is distributed among various ion and excited states. The production rates for these states may be divided into two parts - one produced by direct impact of the beam electrons and the other by impact of secondary electrons. This requires the impact cross sections both at the primary energy and over the energy range important to secondary electron impact processes.

Calculations have been performed for energy deposition in air with primary electron fluxes having energies of 1, 10, 100, and 1000 keV. The easiest part of these calculations is the specification of P_b, the production rates by primary or beam electron impact. P_b is given by

$$P_b^{\ell i} = n_\ell j_b(E_b)\sigma_{\ell i}(E_b) \tag{12}$$

The production rate produced by secondary electron impact $P_s^{\ell i}$ was given previously by Equation (1). The needed secondary electron flux vn_e has been obtained from Equation (2) in its steady state form with the source spectrum given by Equation (3). The time independent results are satisfactory here since our aim is to show how energy becomes partitioned among the various states. For chemistry modeling purposes, however, explicit time dependence is necessary.

Before presenting results from solutions of Equation (2), we wish to note how the energy is distributed in the secondary electron source spectrum. We are thus discussing the behavior of the applied differential ionization cross sections for N_2 and O_2. The purpose for presenting this information is to note how much source energy is not taken into account when Equation (2) is solved over less than the fully allowed secondary electron energy range. This is pertinent to our calculations when the primary energy is above a few

hundred keV since we do not account for secondaries with energies greater than 100 keV. Figure 3 shows the fraction of the initially generated secondary electron energy $f_s(E_s)$ at energies less than E_s for primary energies of 1, 10, 100 and 1000 keV. In each case, the cutoff in f_s comes where E_s is half of the primary energy. This defines the upper limit of E_s. We observe that the high energy tail of the secondary electron source spectrum does contain measurable energy in spite of the fact that the electrons available are insignificant compared to the total number within the spectrum. Figure 4 recasts the information from Figure 3 in terms of the average energy $\langle E_s \rangle$ of the initially produced secondary electrons. At a given energy E_s, $\langle E_s \rangle$ is the average from 0 eV to E_s. The rise in $\langle E_s \rangle$ with increasing energy is somewhat steeper than would be obtained using the Moeller expression for $\sigma(E_b,E_s)$ which varies as E_s^{-2}. This is illustrated in Figure 4 by means of the dashed curve which shows how $\langle E_s \rangle$ varies for E_b = 1 MeV assuming the E_s^{-2} dependence. We now proceed to discuss our results but shall refer back to Figures 3 and 4 for those calculations which have not taken into account all available secondary electron energy.

Examples of the calculated flux $vn_e(E)$ are shown in Figure 5 for E_b = 1 Mev. For these results, the maximum energy treated was 20 keV. Referring back to Figure 3, we are thus accounting for 60% of the available secondary electron energy based on the use of the Porter et al. ionization cross section. The calculated flux has been divided by the primary flux thus giving the units of e/eV-e_p. The spectra shown are for pure N_2 and pure O_2, in each case at standard density. The spectrum for air is similar to that of N_2. The point of calculating the exhibited spectra was to determine the sensitivity of the secondary spectrum to composition changes. This is of interest to us in our chemistry modeling since we do observe compositional changes in the major

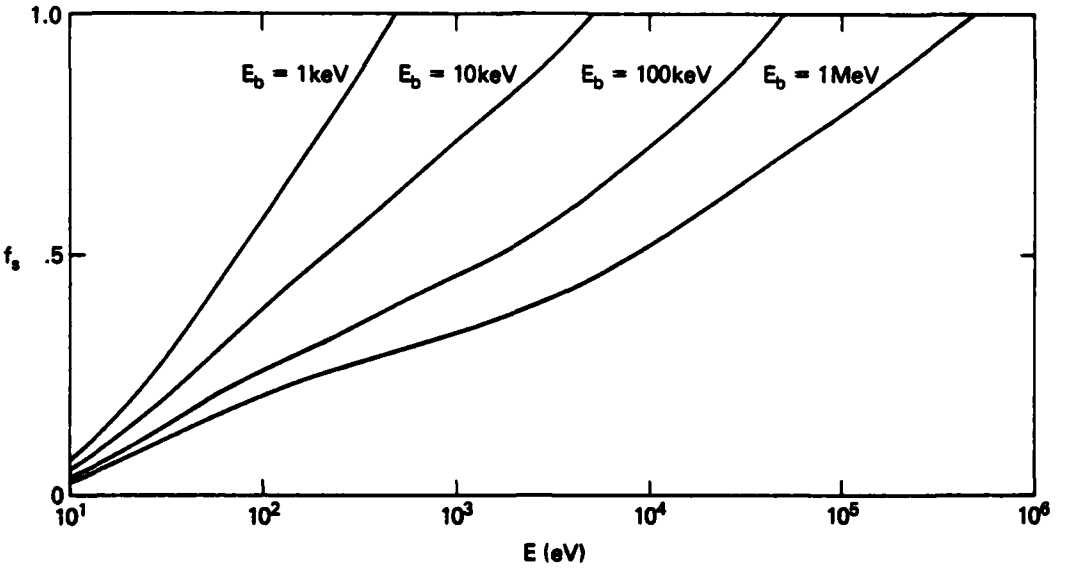

Fig. 3 — Fraction of secondary electron source energy, f_s between O and E_s for primary energies as shown. f_s is based on the ionization cross section of Porter et al[3].

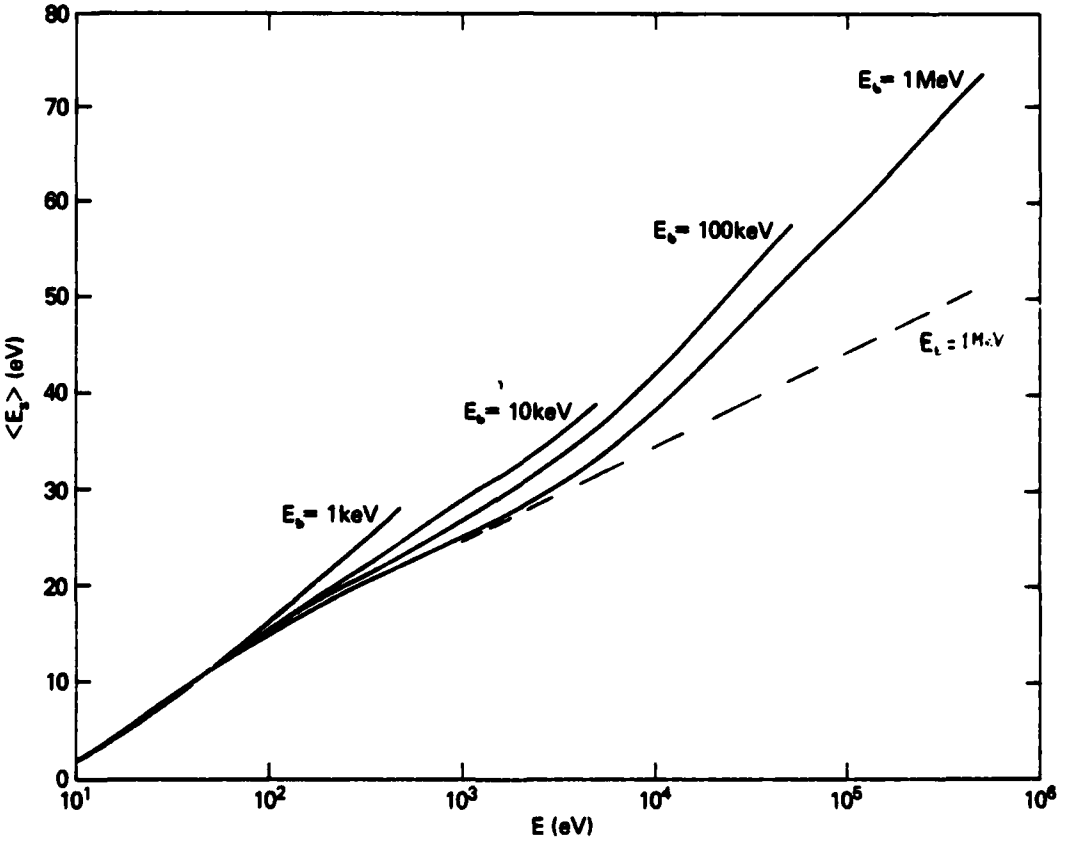

Fig. 4 — Average initial secondary electron energy $\langle E_s \rangle$ obtained using $\langle E_s \rangle = \langle E_s \rangle_{max} f_s(E_s)$ where $\langle E_s \rangle_{max}$ is the average energy over the full range of secondary electron energies. The solid curves were obtained using the ionization cross section of Porter et al[3] while the dashed curve was obtained using the Moeller cross section.

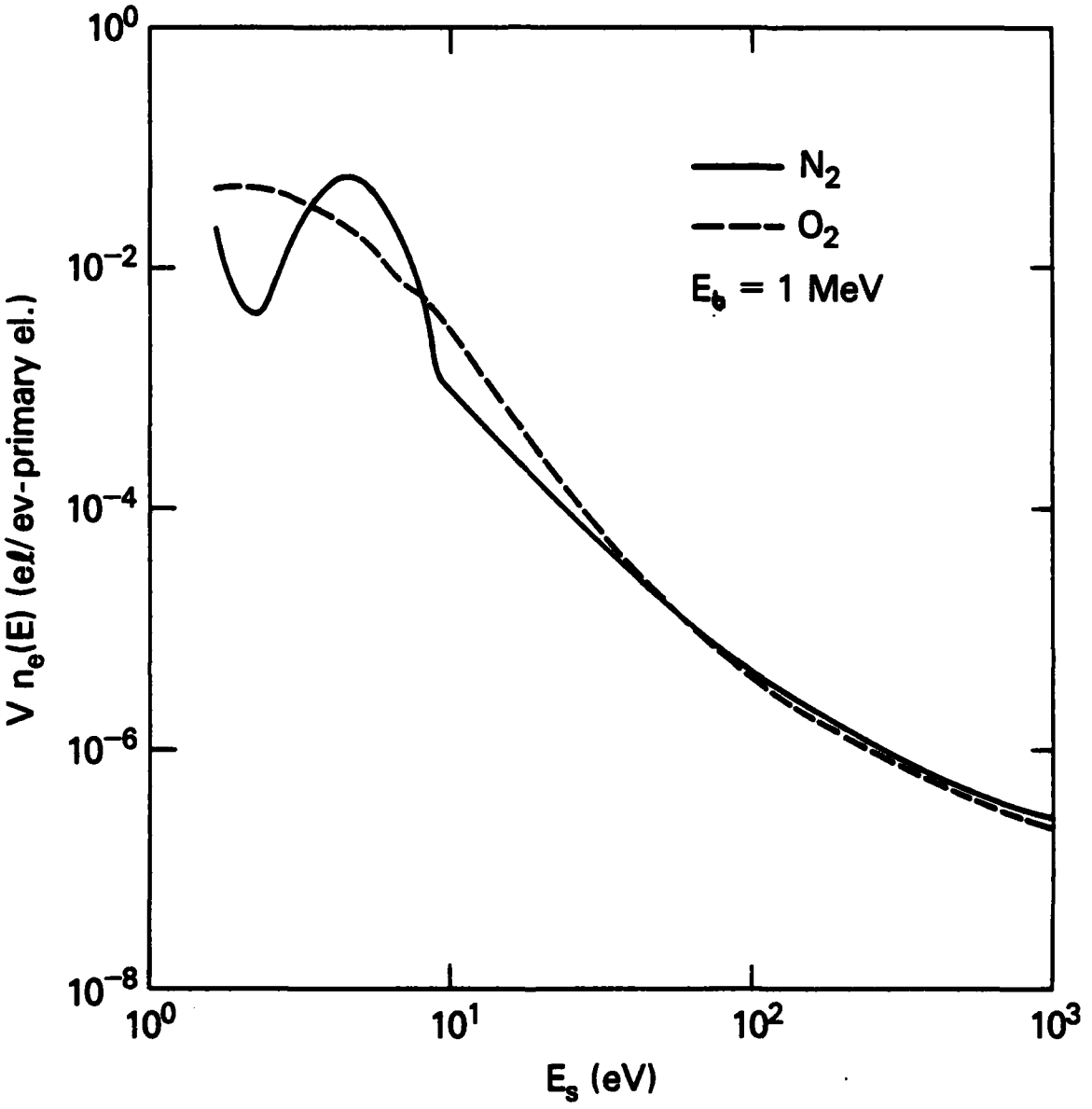

Fig. 5 — Secondary electron fluxes $vn_e(E)$ for pure N_2 and pure O_2 compositions at standard air density. The primary energy is 1 MeV. Secondary electron production has been restricted to less than 20 keV.

constituents for high levels of energy deposition. Based on the results in Figure 5 which apply to the extremes in composition, we can state that compositional changes one might generate in air chemistry modeling will not seriously affect that part of the secondary flux spectrum capable of producing ionization and excitation. It should be noted that the results below ~ 10 eV are sensitive to the amount of plasma present through the derivative term in Equation (2). Furthermore, it is worth noting that the most pronounced difference between the two spectra which occurs at ~ 2.5 eV is caused by differences in vibrational excitation. For N_2, this produces strong energy loss. We shall limit our presentation of secondary flux results to those shown in Figure 5. The shape of the flux in air for other primary energies is similar to that shown for N_2 over the given energy range.

Before proceeding to discuss how the deposited energy becomes distributed among the various states, we wish to add a few comments to those given in Section 7 on ΔW_{ip}. Its explicit form is

$$\Delta W_{ip} = \frac{dE/dx}{P_{ion}/j_b} \tag{13}$$

where dE/dx is the stopping power and P_{ion} is the sum of P_s and P_p. dE/dx here refers to only the deposited energy explicitly treated in Equation (2). Thus, it is less than obtained by the Bethe formula if the maximum secondary electron energy considered is smaller than its maximum allowed value. In that case, we have used the following expression for dE/dx:

$$dE/dx = \sum_{\ell} n_{\ell}\left[\sum_{k} W_{\ell k}\, \sigma_{\ell k}(E_b) + \int_{o}^{E} E_s \sigma_{\ell}(E_b, E_s)\, dE_s\right] \tag{14}$$

where E refers to the largest secondary energy treated, n_ℓ applies to N_2 and O_2, and $W_{\ell k}$ refers to the potential energy of both excited and ion states. We wish to stress that the needed stopping power is the one just discussed since it refers to the actual energy deposition being modeled.

Table 1 gives ΔW_{ip} for the four primary energies considered. For the first 3 cases, dE/dx refers to total energy deposition since the calculations were performed over the full secondary electron energy range. Dissociative ionization as well as direct ionization have been included in P_p and P_s. We observe some variation in ΔW_{ip} but in all cases its value is close to the accepted value of ~ 35 eV/ion pair. There are two possible sources of error in the calculated values of ΔW_{ip}. One is inaccuracies in the calculated flux $vn_e(E)$. The other is in the applied set of cross sections at primary energies needed to specify dE/dx and P_p. If there are inconsistiencies between this set and its counterpart at lower energies used in Equation (2), they will affect the resulting value of ΔW_{ip}. We do observe some error in the calculated secondary flux based on the applied energy conservation test. The error is not serious, however, since the test generally leads to errors of less than 10%.

We note that at 1 MeV, P_p and P_s are comparable whereas Hirsh et al.[18], for example, report relatively larger contributions from P_s in this energy range. They observe P_s to be ~ 2 P_p. We would also obtain approximately this result had we allowed for the energy degradation of the high energy secondaries extending up to 500 keV. Both P_s and dE/dx would increase accordingly leaving ΔW_{ip} unchanged.

We now address the question of what the distribution of energy is among various states of interest. What will be shown is the production rate of various states relative to the total ion production rate P_{ion}. Table 2 gives

Table 1 — Calculated ΔW_{ip} Values and Terms Used to Specify Them

E_p(keV)	$\frac{dE}{dx}$ (eV/cm)	P_b/j_b	P_s/j_b	$\Sigma P_i/j_b$	ΔW_{ip} (eV/ion pair)
1	1.3(5)	2.4(3)	1.2(3)	3.6(3)	36
10	2.4(4)	3.6(2)	3.4(2)	7.1(2)	34
100	4.7(3)	5.7(1)	7.2(1)	1.3(2)	36
1000	1.4(3)	2.3(1)	1.9(1)	4.1(1)	34

Table 2 — Production Given Relative to Total Ionization Production.
The primary energy is 10 keV. Similar values are obtained at the other primary energies considered in this study.

Process	Species	Primary Production	Secondary Production	Total Production
$N_2 + e \rightarrow N_2^+$	N_2^+	.32	.31	.63
$N_2 + e \rightarrow N^+ + N$	N^+	.090	.065	.16
$N_2 + e \rightarrow \begin{Bmatrix} N + N \\ N + N^+ \end{Bmatrix}$	N	.50	.78	1.3
$N_2 + e \rightarrow N_2(A)$	$N_2(A)$	-	.28	.28
" (B)	$N_2(B)$	-	.13	.13
" (C)	$N_2(C)$	-	.059	.059
$O_2 + e \rightarrow O_2^+$	O_2^+	.084	.070	.15
$O_2 + e \rightarrow O^+ + O$	O^+	.037	.027	.064
$O_2 + e \rightarrow \begin{Bmatrix} O + O \\ O + O^+ \end{Bmatrix}$	O	.05	.19	.24

this information broken down into direct production by the primary electrons and production by secondary electrons. The results apply to a primary energy of 10 keV. We have generated these results at the other energies as well and obtain similar values. We observe similar contributions to the total production by primaries and secondaries for the dipole allowed transitions producing the given states. For triplets states, such as $N_2(A^3\Sigma)$, the excitation cross section falls too fast with increasing energy for primary excitation to be important. The total values for ionization and dissociation in Table 2 may be compared with similar ones generated by F. Gilmore, as quoted by Johnston[19], using a continuous slowing down scheme. We observe no serious differences between the two sets of values.

9. SUMMARY

We have presented a computational model for solving an integral equation giving the secondary electron distribution function in the local approximation. Energy loss is treated as discrete which has led us to apply a detailed set of electron impact cross sections. Our application of the model has been to energy deposition in air caused by the passage of energetic primary electrons. Results included the spectrum of secondary electrons under steady state conditions, resulting eV/ion pair values, and the distribution of energy among several states. The calculated eV/ion pair values are close to the universally applied value of ~ 35. The distribution information presented gives one the production of a given state or species by either type of exciting electron-primary or secondary.

REFERENCES

1. A. E. S. Green and C. A. Barth, J. Geophys. Res. 70, 1083 (1965).

2. R. S. Stolarski and A. E. S. Green, J. Geophys. Res. 72, 3967 (1967).

3. H. S. Porter, C. H. Jackman and A. E. S. Green, J. Chem. Phys. 65, 154 (1976) and references therein.

4. P. M. Banks, C. R. Chappell, A. F. Nagy, J. Geophys. Res. 79, 1459 (1974).

5. D. Strickland and P. C. Kepple NRL Memo. Report 2779 (1974).

6. L. G. Peterson, Phys. Rev. 187, 105 (1969).

7. T. E. Cravens, G. A. Victor, and A. Dalgarno, Planet Space Sci. 23, 1059 (1975).

8. J. L. Fox, A. Dalgarno and G. A. Victor, Planet Space Sci. 25, 71 (1977).

9. M. J. Berger and S. M. Seltzer, J. Atm. Terr. Phys. 32. 1015 (1970).

10. M. Walt, W. M. McDonald and W. E. Francis, Physics of the Magnetosphere, Carovillans, et al Eds., Reidel, Dordrecht (1968).

11. D. J. Strickland, D. L. Book, T. P. Coffey and J. A. Fedder, J. Geophys. Res. 81, 2755 (1976).

12. D. R. Shure and J. T. Verdeyen, J. Appl. Phys. 47, 4484 (1976).

13. Y. A. Medvedev and V. D. Khokhlov, Soviet Phys. Tech. Phys. 24, 181 (1979) ibid 185.

14. A. W. Ali and D. J. Strickland (in preparation)

15. C. Moeller, Ann. Phys. 14, 531 (1932).

16. A. W. Ali "Excitation and Ionization Cross Sections for Electron Beam and Microwave Energy Deposition in Air" NRL Memo Report 4598 (1981).

17. R. W. Schunk and P. B. Hays, Planet Space Sci. 19, 113 (1971).

18. M. N. Hirsh, P. N. Eisner and J. A. Slevin, Phys. Rev. 178, 175 (1969).

19. R. Johnston, Task II Studies in Non Equilibrium Air Plasmas -EO and RF Observables Final Report Contract #N60921-75-C-0210, Science Application Incorporated SAI-072-647-PA (1975).

DISTRIBUTION LIST

Chief of Naval Operations
(Attn: Dr. C. F. Sharn (OPO987B))
Washington, D.C. 20350

Air Force Weapons Laboratory
Kirtland Air Force Base
Albuquerque, New Mexico 87117
ATTN: Dr. K. Dreyer
Dr. D. Straw

U.S. Army Ballistics Research Laboratory
Aberdeen Proving Ground, Maryland 21005
ATTN: Dr. D. Eccleshall (DRXBR-BM)

Ballistic Missile Defense Advanced Technology Center
P.O. Box 1500
Huntsville, Alabama 35807
ATTN: Dr. M. Hawie (BMDSATC-1)

B-K Dynamics Inc.
15825 Shady Grove Road
Rockville, Maryland 20850
ATTN: Dr. R. Linz

Lawrence Livermore Laboratory
University of California
Livermore, California 94550
ATTN: Dr. R. J. Briggs
Dr. T. Fessenden
Dr. E. P. Lee
Dr. S. Yu

Mission Research Corporation
735 State Street
Santa Barbara, California 93102
ATTN: Dr. C. Longmire
Dr. N. Carron
Dr. M. Schiebe

National Bureau of Standards
Gaithersburg, Maryland 20760
ATTN: Dr. Mark Wilson

Science Applications, Inc.
Security Office
5 Palo Alto Square, Suite 200
Palo Alto, California 94304
ATTN: Dr. R. R. Johnston
Dr. Leon Feinstein
Dr. D. Keeley

Naval Surface Weapons Center
White Oak Laboratory
Silver Spring, Maryland 20910
ATTN: Mr. R. J. Biegalski
Dr. C. M. Huddleston
Dr. M. H. Cha
Dr. H. S. Uhm
Dr. R. B. Fiorito
Dr. R. Cawley

C. S. Draper Laboratories
Cambridge, Massachusetts 02139
ATTN: Dr. E. Olsson
Dr. L. Matson

Physical Dynamics, Inc.
P. O. Box 1883
La Jolla, California 92038
ATTN: Dr. K. Brueckner

Office of Naval Research
Department of the Navy
Arlington, Virginia 22217
ATTN: Dr. W. J. Condell (Code 421)
Dr. T. Berlincourt (Code 464)

Avco Everett Research Laboratory
2385 Revere Beach Pkwy.
Everett, Massachusetts 02149
ATTN: Dr. R. Patrick
Dr. Dennis Reilly

Defense Technical Information Center
Cameron Station
5010 Duke Street
Alexandria, VA 22314 (12 copies)

Naval Research Laboratory
Washington, D.C. 20375
ATTN: M. Lampe - Code 4792
J. R. Greig - Code 4763
T. Coffey - Code 4000
S. Ossakow - Code 4700 (26 copies)
Library - Code 2628 (20 copies)
A. W. Ali - Code 4700.1 (30 copies)
B. Hui - Code 4790
M. Piccone - 4040

Defense Advanced Research Projects Agency
1400 Wilson Blvd.
Arlington, Virginia 22209
ATTN: Dr. J. Mangano
Major R. Gullickson

JAYCOR
205 S. Whiting St.
Alexandria, Virginia 22304
ATTN: Drs. D. Tidman
R. Hubbard
S. Slinker

Mission Research Corp.
1720 Randolph Road, S.E.
Albuquerque, NM 87106
ATTN: Dr. Brendan Godfrey
Dr. L. Wright

Pulse Sciences, Inc.
1615 Broadway, Suite 610
Oakland, CA 94612
ATTN: Dr. S. Putnam

McDonnell Douglas Research Laboratories
Dept. 223, Bldg. 33, Level 45
Box 516
St. Louis, MO 63166
ATTN: Dr. Michael Greenspan
Dr. C. Leader

Prof. David Hammer
Laboratory of Plasma Studies
Room 290
Grumman Hall
Cornell University
Ithaca, NY 14853

Sandia Laboratories
Albuquerque, NM 87185
ATTN: Dr. Bruce Miller
Dr. Barbara Epstein
Dr. John Olsen
Dr. Don Cook

Beers Associates, Inc.
P. O. Box 2549
Reston, VA 22090
ATTN: Dr. Douglas Strickland

R and D Associates
P.O. Box 9695
Marina del Rey, California 90291
ATTN: Dr. F. Gilmore

Director
Defense Nuclear Agency
Washington, D.C. 20305
ATTN: Dr. C. Fitz (RAAE)
Dr. P. Lunn (RAAE)

Los Alamos National Laboratory
(Attn: Dr. H. O. Dogliani)
Mail Station 5000
P. O. Box 1663
Los Alamos, NM 87545

Los Alamos National Laboratory
(Attn: Dr. Thomas P. Starke)
Mail Stop 942
P. O. Box 1663
Los Alamos, NM 87545

END

FILMED

1-83

DTIC